Design of Bifurcated Beam using Convex Bent Array Feed for Satellite Mobile Earth Station Application

Zanurlida TENGAH [1], Nurul Huda ABD RAHMAN [1], Yoshihide YAMADA [2,3], Nur Emileen ABD RASHID [4], Idnin PASYA [4], Mohd Aziz ARIS [5], Nguyen Quoc DINH [6]

[1] Antenna Research Centre (ARC), School of Electrical Engineering, College of Engineering, Universiti Teknologi MARA, 40450 Shah Alam, Selangor, Malaysia
[2] Malaysia-Japan International Institute of Technology (MJIIT), Universiti Teknologi Malaysia, 54100 Kuala Lumpur, Malaysia
[3] National Defense Academy, Yokosuka, Kanagawa, Japan
[4] Microwave Research Institute, Universiti Teknologi MARA, 40450 Shah Alam, Selangor, Malaysia
[5] School of Electrical Engineering, College of Engineering, Universiti Teknologi MARA Caw. Terengganu, 23000 Dungun, Terengganu, Malaysia
[6] Faculty of Radio-Electronic Engineering, Le Quy Don Technical University, Hanoi, Vietnam

zanurlida@yahoo.com, {nurulhuda0340, emileen98, idnin, mohda474}@uitm.edu.my, yoshihide@utm.my, dinhnq@lqdtu.edu.vn

Submitted January 26, 2022 / Accepted September 6, 2022 / Online first November 7, 2022

Abstract. *For multibeam operation at the satellite mobile earth station and telecommunication base stations, a cylindrical lens antenna with multi-feed is a promising candidate due to the simple antenna configuration and good scanning performance to produce multi beams. However, efficient illumination at the lens surface is critical. Previously, the present antennas were used; however, a significant tapered distribution is observed, resulting in under-illumination at the lens edges. The feed positions are requested to be placed near the lens to achieve a slender lens form. Therefore, the feed radiation pattern should have high radiations at the wide-angle region. This paper proposes a bifurcated beam array antenna to alter the amplitude distribution. This method is expected to improve the radiation pattern coverage area. In designing a bifurcated beam antenna, the important parameter is to ensure that the separated beams have the same current phase excitations at each radiating element and a precise patch arrangement to achieve the targeted radiation pattern. The differences in surface current will affect the radiation patterns due to the significant interference and cancellation effects which will contribute to high losses. This paper forms the array by a convex bent array with the same phase excitation for all patch elements. The feed performances are also verified by the good agreement between simulated and measured results. An improved aperture distribution is demonstrated for array feed having $0.7\lambda_o$ spacing compared to the tapered distribution by a single patch design with the hyperbolic lens through detailed analysis and comparative study. By changing the spacing distance of the convex bent array, many radiation patterns are observed, such as strong radiation in the wide-angle region, the uniform radiation level in a wide-angle region, and the tapered radiation pattern. Thus, many aperture distributions of center-dip, uniform and tapered, are achieved.*

Keywords

Multibeam, satellite mobile earth station, cylindrical lens antenna, bifurcated beam, convex bent array

1. Introduction

For future satellite earth station and telecommunication base station systems, the multibeam operation becomes highly demanded to ensure consistent communication to many users within a wide coverage area [1]. An antenna system with numerous beam capabilities and multi-frequency is required in the satellite mobile earth station system, as shown in Fig. 1 [2–4].

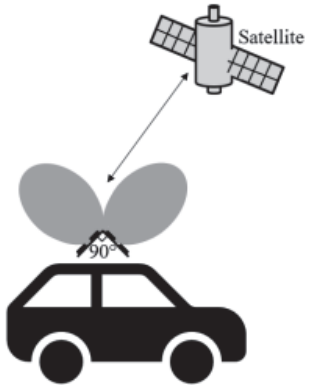

Fig. 1. Satellite mobile earth station configuration.

DOI: 10.13164/re.2022.0541

The main objectives of the multibeam are to maximize the frequency reuse, pattern roll-off outside of the spot-beam, minimum gain over the coverage region by increasing the number of antennas at the base station and minimizing the side lobe radiation [5], [6]. In the satellite mobile communication systems, the multibeam also effectively increases the signal power flux density of the earth station by narrowing the beamwidth pattern. The increase of signal power flux density has an advantage, where the transmission capacity can be increased; thus, it can reduce the earth station size and be more economical [7]. For mobile earth and telecommunication base stations, conventional feed radiators such as horn, dipole, and phased array antennas have been used in the previous generation of mobile technology. However, those antennas are unsuitable for the mobile system due to the higher capacity requirement.

Many multibeam antennas have been designed, such as phased arrays, reflectors, and dielectric lens antennas. Phased array antennas were designed to efficiently produce beam steering characteristics at different scanning angles [8, 9]. However, these array circuits are complex in design, specifically the feeding network composed of the power dividers and phase shifters, which will contribute to high feeder loss and limit the usage of wideband frequency [10–12]. Previously, a linear array antenna was also employed as the feed radiator. The array elements were divided into sub-arrays, and each sub-array consisted of array elements connected by feeding cables. Thus, large spaces are required to accommodate the feeding cables, especially for multi-frequency applications [10]. These feeding circuits have also contributed to feeding losses, and thus, the existing linear array antenna should be reconsidered for the multi-frequency and multibeam applications [5], [12].

Multi-feed antennas are used in reflector and lens antenna systems to achieve multibeam features. Nowadays, the lens antenna has received good attention from researchers due to its beam stability and high directivity, especially for wide-angle beam scanning and multibeam application [13]. Previous researchers [14] have proven that the omnidirectional pattern diversity can be accomplished by applying a graded dielectric lens antenna. Multiple equally spaced beams are radiated by the lens when an accurate phase is excited. However, this method has increased the design and fabrication complexity of the lens structure, and the amplitude distribution remains strongly tapered, resulting in narrow coverage areas.

A lens antenna is usually made from low refractive index material that can minimize the reflection at the lens surface. It has no aperture blockage issue caused by the feed radiator and can be designed to have low sidelobe levels [13–21]. There are many types of lens antennas with different characteristics. Cylindrical lens antennas are usually used for beam scanning with single or multiple feed possibilities [22], [23]. Due to the symmetrical features and excellent focusing properties, a cylindrical lens antenna is an attractive solution that can exhibit a narrow beam shape and multibeam capacity [24]. In a multi-feed lens system, the array feed arrangement should be determined to ensure efficient waves illumination from feed radiators to the lens area. Thus, a bifurcated beam radiation pattern was proposed to alter the tapered amplitude distribution produced by a single beam. A set of dipole antennas can produce the bifurcated beam. However, when multiple dipoles are arranged in parallel, the phase directions of all dipoles are not the same. This arrangement has affected the formation of the total radiation pattern due to the significant interference and the cancellation effects [25]. A phased or scanning array antenna can also produce multiple beams where the phase excitation of each element can control the main beam. However, it requires a complex feed network, resulting in higher losses and reduced efficiency [26–31]. The electric field vectors produced by this antenna are also in different vectors orientation that caused the amplitude degradation.

This paper proposes a convex bent array for the cylindrical lens antenna to produce a bifurcated beam with the same electric field vectors orientation, as shown in Fig. 2. The bifurcated beam antenna is proposed because the dual beams can be produced using one feed radiator, where the bifurcated beam can also cover the lens edge. Besides that, this design also has a simple antenna configuration because the antenna is not composed of many feeding networks compared to the previous antenna design, which can affect the high losses and low efficiency of the antenna design. Besides that, the phase distribution of this antenna is expected to be in the same current flow direction, where there is no significant interference and cancellation effect happens after the signal pass through the lens structure. The lens is formed cylindrically around the vertical axis (z-axis) and is placed in front of the multi-feed radiator. For installation convenience on a base station, the distance between feeds to the lens should be as close as possible, generally at the lens focal point along the lens axis, to ensure that the feed signal is entirely directed to the lens. Hence, no significant gain reduction for all the beam scanning angles [8], [9].

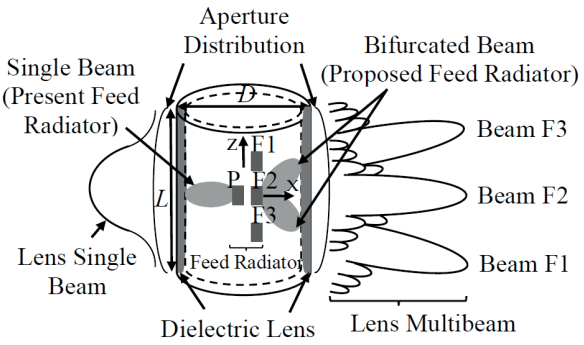

Fig. 2. Existing and proposed configuration of a cylindrical lens antenna.

2. Antenna Configuration

This paper demonstrates a 1.72 GHz bent array antenna design to produce a bifurcated beam radiation pattern to increase the maximum beam angle from feed to the lens edge. As for beam shaping by the lens, the relation between array element numbers, N, and beam shape was investigated. A Matrix Laboratory (MATLAB)® program [32] was developed to calculate the N based on the array configuration shown in Fig. 3. $E_p^2(\theta)$ is the electric field intensity of the feed radiator given by (1). θ_s indicates the beam shift angle, and m is the beam sharpness controlled by the radiated beam, which is the parameter to determine the beamwidth.

$$E_p^{\,2}(\theta) = \left\{\cos(\theta - \theta_s)\right\}^m \tag{1}$$

The bent array antenna configuration that can produce a bifurcated beam shape is shown in Fig. 3(b), where the θ_w, d, and $AF(\theta)$ indicate the bent angle, spacing between array elements, and array factor, respectively. These parameters are related by (2) and (3). As for the antenna configuration, the relation of the θ_w and θ_s is expressed by (4):

$$AF(\varphi) = \frac{\sin\dfrac{N\varphi}{2}}{N\sin\left(\dfrac{\varphi}{2}\right)}, \tag{2}$$

$$\varphi = \beta d\sin\theta_0 = \frac{2\pi}{\lambda}d\sin\theta_0, \tag{3}$$

$$\theta_w = 180 - 2\theta_s \text{ [deg]}. \tag{4}$$

From the previous work by the authors [6], to determine the N, the $AF(\theta)$ should have a similar beam shape as the $E_p^2(\theta)$. Comparison and analysis of various configurations and parameters have been made in MATLAB before further validation works in Computer Simulation Technology (CST) Studio Suite® tool [33]. Based on the result, $N = 2$ and $m = 2$ produced an excellent radiation pattern that agrees with the $AF(\theta)$. From the calculated result, the desired $\theta_s = 45°$ can be produced by the array structure of $N = 2$ and $d = 0.7\lambda_o$. Thus, further validation of the proposed bent array structure is done through electromagnetic simulation in this paper. The final system consists of four microstrip patch elements with a serial feed line network connected with a 180° phase difference, ΔP between elements.

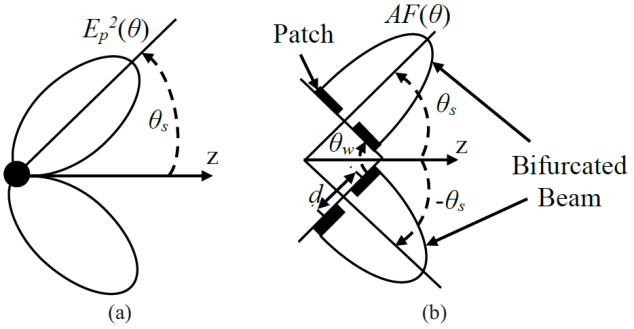

Fig. 3. Bifurcated beam antenna: (a) bifurcated beam, and (b) convex bent array configuration ($\theta_w = 90°$).

3. Bent Antenna Design

To produce $\theta_s = 45°$ by bifurcated beam radiation, the bending angle of the bent array structure θ_w should be 90° by referring to (4). A single patch, a 4×1 array, and a convex bent array with a serial feed network are simulated and validated using CST software in this study.

3.1 Single Patch and Bent Array Design

Figure 4 shows a single patch antenna simulation model consisting of a microstrip patch on the top, dielectric substrate, and ground plane at the bottom. The dielectric constant, ε_r, and loss tangent of the substrate, δ RO5880, are 2.2 and 0.0009, respectively. The substrate width, W_s, and length, L_s are the same, which is 117.4 mm with a thickness, h of 1.57 mm. The patch element width, W_p length, L_p, and copper thickness, t_c are 55.6 mm, 56.5 mm, and 0.035 mm.

The simulated results of the antenna are shown in Fig. 5. Figure 5(a) shows that the antenna resonates at the desired frequency of 1.72 GHz with a good return loss of –27.11 dB and impedance bandwidth of 28.3 MHz. Figure 5(b) shows the radiation pattern of the single patch antenna in the E-plane, with an excellent gain, G of 5.96 dB.

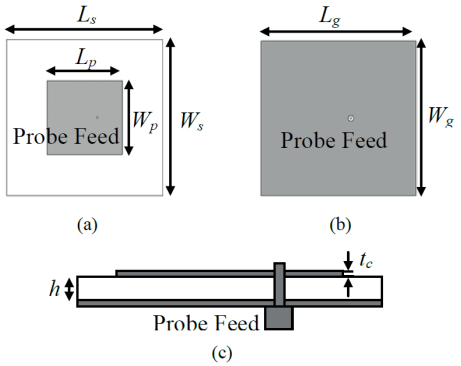

Fig. 4. Simulation model of a single patch antenna structure; (a) top view, (b) bottom view, and (c) side view.

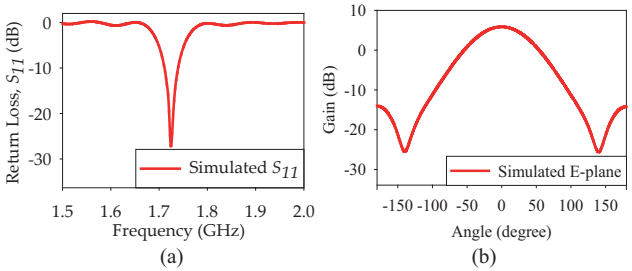

Fig. 5. Simulated results of the single patch antenna: (a) Return loss, and (b) E-plane radiation pattern in Cartesian view.

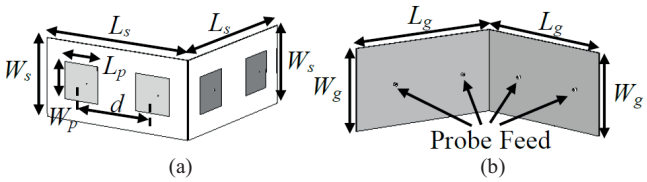

Fig. 6. Simulation model of a convex bent array antenna with a coaxial probe feed at each patch: (a) Top view, and (b) bottom view.

The antenna also has a good directivity, D of 7.80 dBi with an efficiency, η of 65.45%.

Then, to demonstrate the ability of a bent array to produce a bifurcated beam, the single patch antenna was arranged in an array structure using $N = 2$ as derived previously in Sec. 2. Figure 6 shows the bent array structure with $\theta_w = 90°$ that consists of four probe-fed patch elements, with two elements on each side.

Figure 7 shows the radiation pattern of the convex bent array for various spacing distances, d to determine the optimum element spacing that can produce an excellent and balanced bifurcated beam shape. As theoretically predicted by (4), two beams are produced at 45° and –45°, respectively. From the simulated radiation patterns for different d, $d = 0.7\lambda_o$ gives a good bifurcated beam shape where the two beams are clearly separated compared to other d values. This finding is consistent with the theoretical modeling done using MATLAB, as stated in Sec. 2.

Several bent array angles have been analyzed to prove the relation shown by (4) using MATLAB software from the previous work. Figures 8(a), (b), and (c) show the simulated E-plane radiation pattern of bent array antenna for $d = 0.7\lambda_o$ with various θ_w.

Based on the figures, the relation between θ_w and θ_s of all bent array antennas is proven. For example, when θ_w is 60°, the angle of θ_s becomes 60° for $N = 2$ and $N = 3$. For $\theta_w = 90°$ and 270°, two beams are produced at –45° and 45° respectively for $N = 2$ and $N = 3$. From these patterns, it shows that the increment of θ_w has decreased the θ_s. Therefore, to increase θ_s, the θ_w should be reduced, and the relation between θ_s and θ_w can be considered in designing a lens antenna to reduce the diameter of the lens structure. The figures also show that $N = 2$ produces better beam shape performance than $N = 3$, consistent with the MATLAB result, which is important in the validation process of this research. In addition, as shown in Fig. 8, the side

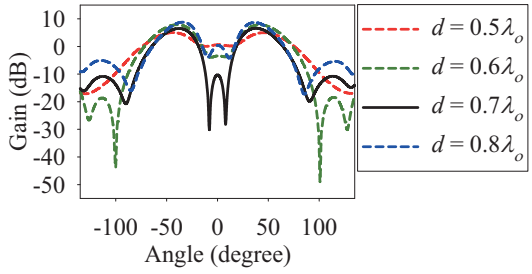

Fig. 7. Simulated E-plane radiation pattern of a convex bent array antenna with various d values.

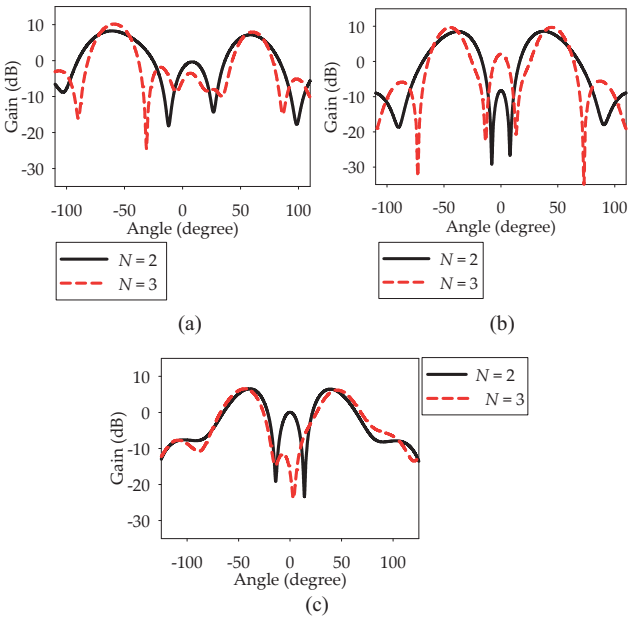

Fig. 8. Simulated E-plane radiation pattern of bent array antenna for $d = 0.7\lambda_o$ with various θ_w and N values: (a) θ_w = 60 degree, (b) θ_w = 90 degree, and (c) θ_w = 270 degree.

lobes of all the radiation patterns for $N = 3$ designs are bigger than the side lobes of $N = 2$ designs, where normally, when the beamwidth decreases, the side lobe is increased. Besides that, the middle lobe produced by $N = 3$ is not bigger than $N = 2$, where it should be reduced.

3.2 Bifurcated Beam Antenna with Feed Network

3.2.1 Feed Line Optimization of a 4×1 Array

Next, a 4×1 array antenna with a serial feedline network is designed. Figure 9 shows the 4×1 array antenna, fed by a coaxial probe. The 4×1 array dimensions are shown in Tab. 1.

Figures 10(a), (b), (c), (d), and (e) show the calculation results of electric-field intensity, magnetic field, phase distribution, and surface currents for the 4×1 array. Figure 10(a) indicates the correlation of the electric field inten-

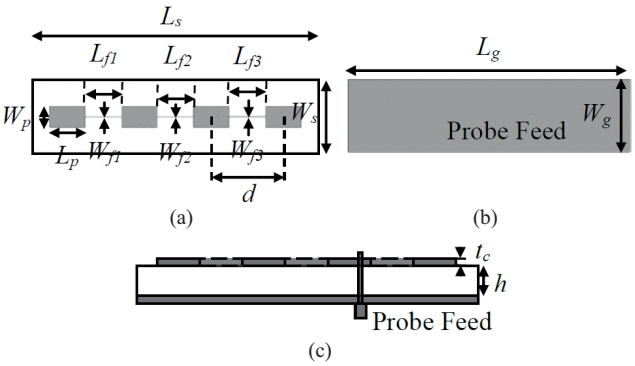

Fig. 9. Simulation model of a 4×1 array antenna structure: (a) Top view, (b) bottom view, and (c) side view.

Parameter	Dimension [mm]
W_s	117.4
L_s	455.9
W_p	35.0
L_p	57.8
d	$0.7\lambda_o$
W_{f1}	1.0
W_{f2}	0.8
W_{f3}	1.2
L_{f1}, L_{f2}, L_{f3}	58.7
h	1.57
t_c	0.035

Tab. 1. Dimension of 4×1 array antenna.

sity to the impedance at each element, where the center elements have lower impedance than the elements at the edges. This trend in E-field intensity is inversely proportional to the current amplitude, as shown in Fig. 11(a). The maximum and minimum electric fields in Fig. 10(b) can be seen on the left and right sides of the radiating patches [28]. Figure 10(d) shows the uniform phase distribution of the antenna at each patch element for a 4×1 array. Theoretically, the antenna's phase is affected by the feedline length of the antenna structure. As can be seen in the graph, the phase has a uniform distribution. Thus, the feedline length dimension is not optimized. In addition, the uniform phase also can be proven by the same current flow direction of each patch element, as shown in Fig. 10(e). As shown in Fig. 10(e), the current amplitude for each patch surface,

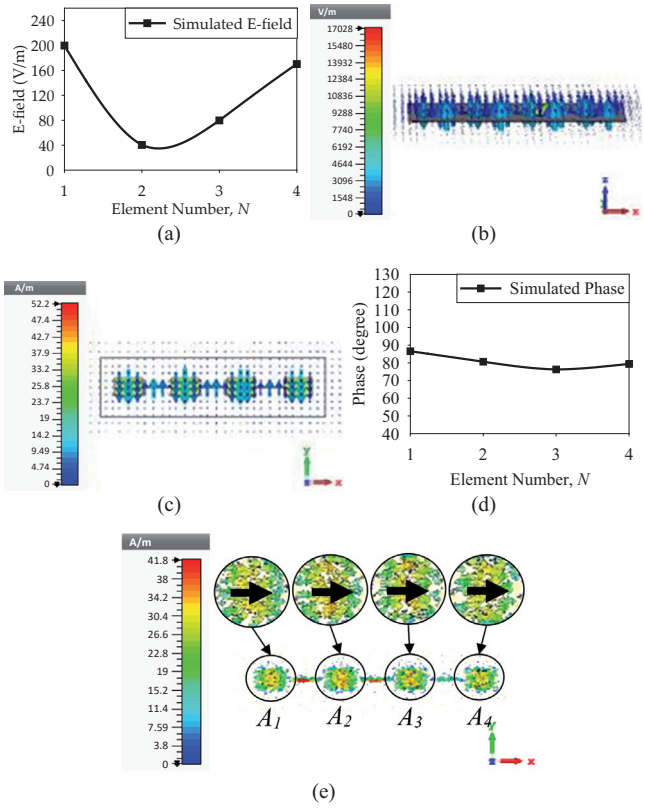

Fig. 10. Near field intensity of 4×1 array: (a) Electric field at each radiating elements, (b) electric field (side view), (c) magnetic field (top view), (d) phase distribution, and (e) surface current in transparent view (top view).

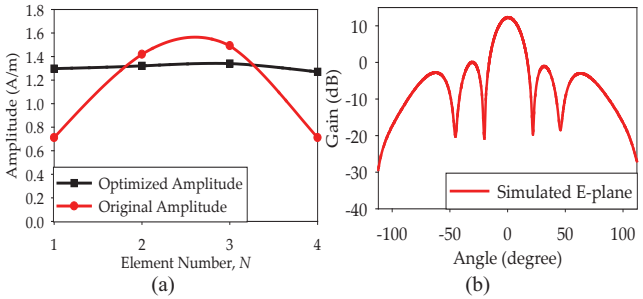

Fig. 11. Simulated results for 4×1 array antenna structure: (a) Amplitudes of currents, and (b) E-plane radiation pattern in Cartesian view.

labeled as A_1, A_2, A_3, and A_4, has the same orientation. It is crucial to ensure that all currents add up in phase to avoid gain and efficiency degradation contributed by the losses [29].

The current amplitude of each patch was originally not uniform, which affects the radiation pattern performance when designing the bifurcated beam antenna. Due to the 4×1 flat configuration, the array antenna cannot be fed from the center of the structure, which has caused an unbalanced current amplitude and radiation pattern results, as shown in Fig. 11(a). Thus, an iterative process was performed to optimize the serial feed line of the patch array antenna through adjustments to the width of the feed lines to achieve a uniform current amplitude with a balanced bifurcated beam radiation pattern. The modification of the feed lines has altered the intensities around the patch, resulting in consistent current amplitudes for each patch surface, as seen in Fig. 11(a).

This process is essential during implementing the bifurcated beam for the bent array to ensure that the bifurcated beam is balanced in shapes. The simulated radiation pattern of the 4×1 array antenna is shown in Fig. 11(b).

3.2.2 Substrate Optimization of a Convex Bent Array Antenna

The 4×1 array antenna with serial feedline structure is bent to produce a bifurcated beam. Figure 12 shows the simulation model of a convex bent array. The antenna structure is bent with an angle of 90° in between the two segments. Slight modifications were made to the initial antenna size by adjusting the radiating element length to obtain resonance at the desired frequency. The final dimensions of the antenna length for both planes are 227.9 mm and 226.4 mm, respectively.

However, the required shifting angle, θ_s of 45° for the bifurcated beam, was not achieved. Therefore, to solve this problem, the fringing effect concept was adopted by extending the size of the substrate and ground to improve the θ_s performance. Hence, an extended convex bent array antenna was designed, with an extended substrate and ground length dimension denoted as ΔS in Fig. 12. The fringing effect method created fringing fields at the edge of the patches to produce wider θ_s [30]. The ΔS of substrate and ground for both sides are 45 mm.

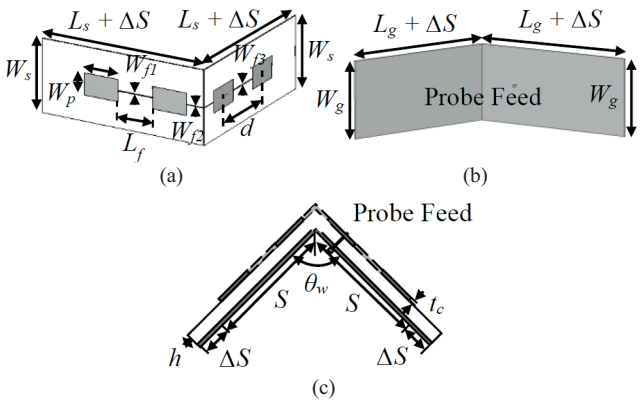

Fig. 12. Simulation model of a convex bent array antenna with serial feed network: (a) Top view, (b) bottom view, and (c) side view.

The electric-field intensity of the convex bent array is shown in Fig. 13. From Fig. 13(a), the electric field intensities are consistent for all four patches, almost similar to the previous 4×1 array. The three-dimensional electric and magnetic field distribution views are presented in Fig. 13(b) and (c), respectively. From the figures, the electric and magnetic field distribution have the same current flow direction for each patch surface at one time. The phase distribution for the convex bent array is shown in Fig. 13(d). The plotted graph shows that this structure also has an almost uniform phase distribution, the same as the 4×1 array structure. Thus, the feedline length of this structure

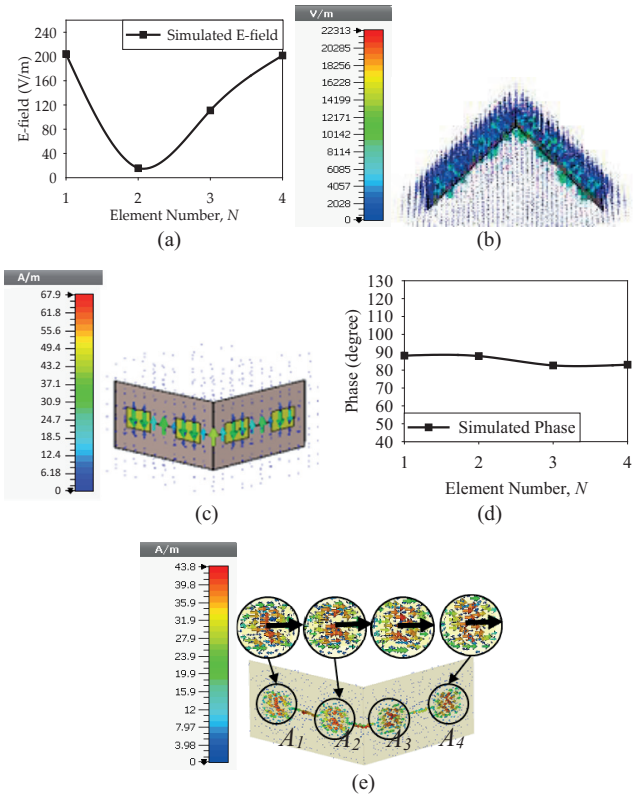

Fig. 13. Near field intensity of convex bent array antenna: (a) Electric field at each radiating elements, (b) electric field (side view), (c) magnetic field (top view), (d) phase distribution, and (e) surface current in transparent view (top view).

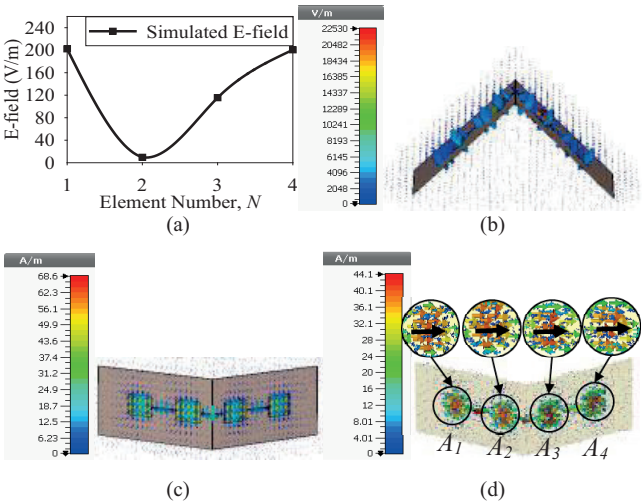

Fig. 14. Near field intensity of extended convex bent array antenna; (a) electric field at each radiating elements, (b) electric field (side view), (c) magnetic field (top view), and (d) surface current in transparent view (top view).

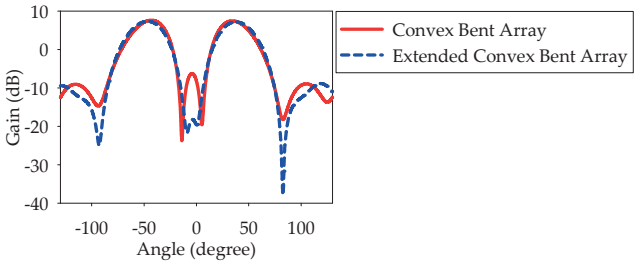

Fig. 15. Comparison of simulated E-plane radiation pattern for convex bent array and extended convex bent array in Cartesian view.

is also not optimized since it has already produced a uniform phase distribution. The calculation results of the surface current for this antenna design in the top view are shown in Fig. 13(e), where the surface current for each patch has the same current direction as the previous design. Figure 14 shows the calculation results of the near field intensity for an extended convex bent array antenna. The electric field, magnetic field, and surface current distribution are almost similar to the previous design, as shown in Fig. 14(a), (b), (c), and (d).

The comparison of gain for the convex bent array and the extended convex bent array is discussed based on the simulated E-plane radiation pattern, as shown in Fig. 15.

In terms of θ_s, the extended convex bent array was increased from 38.20° to 42.5° after the extension work. Furthermore, as shown in the graph, the middle section of bifurcated beams for extended convex bent array also is smaller. This scenario is due to the decrease in the mutual coupling between the bent structures, especially at the bending area.

3.3 Lens Antenna Performances

The proposed convex bent array is to be used as a feed radiator for a dielectric lens antenna in a mobile base

station application. The relation between the feed radiation pattern ($E_p^2(\theta)$) and the electric power distribution ($E_d^2(x)$) on the aperture plane is shown in Fig. 16. Based on the figure, the focal length, lens thickness, and lens diameter are indicated as F, T, and D, respectively. During operation, rays coming to the lens are refracted at S_1 and S_2. The ray emitted from the feed at an angle θ reaches S_1 at the point indicated by (x_1, y_1). After passing through the lens, all rays become parallel to the x-axis, suggesting that a flat wavefront is formed.

The lens is called the hyperbolic lens, and the lens surface is given by (5). The hyperbolic lens is chosen because of its simple shape and design [34].

$$r = \frac{(n-1)F}{n\cos\theta - 1} \tag{5}$$

The central thickness of the lens structure, T, is calculated using (6)

$$T = \frac{1}{n+1}\left[\sqrt{F^2 + \frac{(n+1)D^2}{4(n-1)}} - F\right]. \tag{6}$$

Here, n is the refractive index, and r is the distance from the feed to the lens surface. The electric power relation of $E_d^2(x)$ and $E_p^2(\theta)$ is expressed by (7) based on the electric power conservation law

$$E_p^{\,2}(\theta)\,\mathrm{d}\theta = E_d^{\,2}(x)\,\mathrm{d}x\,. \tag{7}$$

To obtain the functional relation, the $\mathrm{d}x/\mathrm{d}\theta$ is calculated. In Fig. 16, x is expressed by (8)

$$x = r\,\sin\theta = \frac{(n-1)F\,\sin\theta}{n\,\cos\theta - 1}. \tag{8}$$

Then, the $\mathrm{d}x/\mathrm{d}\theta$ is obtained as follows:

$$\frac{\mathrm{d}x}{\mathrm{d}\theta} = F\frac{(n-1)(n-\cos\theta)}{(n\cos\theta-1)^2}. \tag{9}$$

By inserting equation (9) in (7), the aperture distribution, $E_d^2(x)$, is determined by (10):

$$E_d^{\,2}(x) = E_p^{\,2}(\theta)\frac{(n\cos\theta-1)^2}{F(n-1)(n-\cos\theta)}. \tag{10}$$

The function $f(\theta)$ shown in (11) is considered to understand the numerical relation of $E_p^2(\theta)$ and $E_d^2(x)$:

$$f(\theta) = \frac{(n\cos\theta-1)^2}{(n-1)(n-\cos\theta)}. \tag{11}$$

For n = 3, then $f(\theta)$ change is shown in Fig. 17. As a result, the aperture distribution, $E_d^2(x)$, is obtained by multiplying Fig. 7 and Fig. 17.

Validation works were performed by comparing the aperture distribution of the single patch and the extended convex bent array antennas when both structures are integrated with a hyperbolic lens structure, as shown in Fig. 16. The purpose of using the bifurcated beam is to modify the aperture distribution for the case when the feed position is located near the lens, especially in the base station antenna configuration.

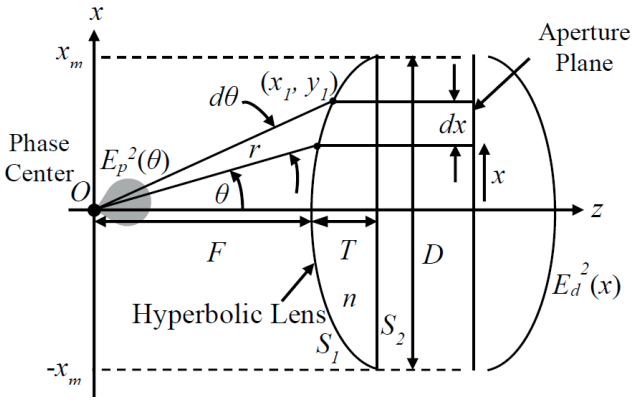

Fig. 16. Lens antenna parameters.

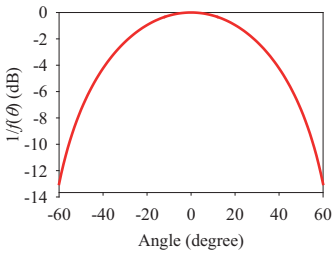

Fig. 17. $1/f(\theta)$ distribution.

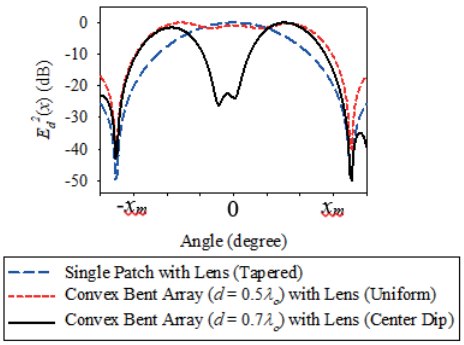

Fig. 18. Aperture distribution of various feed configurations.

For that configuration, the single patch is not suitable for being used as the feed because it will produce a radiation beam with a significant edge taper, resulting in non-uniform illumination of the lens. The expected aperture distributions $E_d^2(x)$ are shown in Fig. 18. Here, the radiation patterns of Fig. 7 are converted to the uniform and the center-dip distributions represented by a single patch, a convex bent array with $d = 0.5\lambda_o$ and $d = 0.7\lambda_o$, respectively. The tapered distribution is for the single patch feed. The radiation pattern concept is expressed in Fig. 19. Compared to the uniform aperture distribution, the radiation level of the tapered distribution is significantly smaller. Based on this distribution, lens illumination is not optimized. In the center-dip distribution, the sidelobe levels are

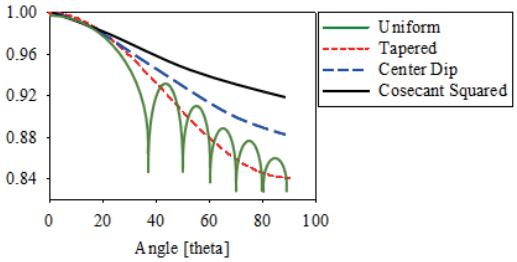

Fig. 19. Radiation patterns of various feed configurations.

increased compared to the uniform distribution [35]. Ideally, the cosecant squared radiation pattern is suitable for the mobile base station because the constant power density can be received at any distance. It is observed that the sidelobe level of the center-dip case is approaching the cosecant squared level. Based on the data, the extended convex bent array with $d = 0.7\lambda_o$ is demonstrated to produce better aperture distribution with high lobe magnitude even at the sides. This observation indicates that efficient lens illumination is achieved. Therefore, the convex bent array pattern of $d = 0.7\lambda_o$ is selected for practical use.

4. Measurement Results

In this section, the 4×1 linear array, convex bent array, and extended convex bent array were fabricated and measured to verify the accuracy of the bifurcated beam array antenna.

4.1 Fabrication and Measurement Method

The antennas were fabricated using a high-precision microstrip circuit plotter, LPKF ProtoMat. Then, the antenna performances and characteristics were verified through laboratory measurements. The Rohde & Schwarz ZVB20 Vector Network Analyser (VNA) with a frequency range of 10 MHz–20 GHz was used to measure the S-parameters. While the OTA-500 Atenlab anechoic chamber is used to measure the radiation pattern, gain, directivity, and efficiency. This anechoic chamber can measure an antenna with a frequency range of 700 MHz to 18 GHz.

Figures 20(a) and (b) show the fabricated 4×1 array and convex bent array antenna. Figures 21(a) and (b) show the measurement configurations of the extended convex bent array antenna in the anechoic chamber. All antennas were measured in vertical positions.

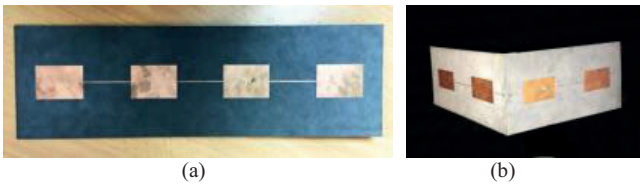

(a) (b)

Fig. 20. Fabricated antennas: (a) Patch array with serial feedline, and (b) convex bent array.

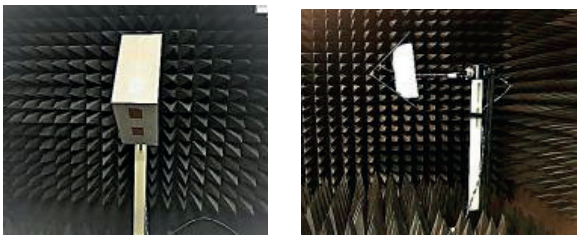

(a) (b)

Fig. 21. Measurement setup of the extended convex bent array: (a) Front view, (b) side view.

4.2 Results and Discussion

This section presents the measurement results of all antennas. During analysis, the simulation and measured results are discussed and compared in terms of the resonant frequency, return loss, bandwidth, gain, directivity, efficiency, and radiation pattern.

4.2.1 Patch Array with the Serial Feed Line

Figure 22 compares simulated and measured return loss for the 4×1 array. The measured return loss slightly shifted to about 0.017 GHz from the simulated data based on the graph with a small percentage of 0.99%. However, this value is considered acceptable in this work because the frequency is still within the range of the actual operating bandwidth for a base station. The difference between the simulation and measurement results is due to the fabrication tolerance and possible inaccuracies during antenna assembly. These factors have contributed to the slight difference in antenna impedance, thus has affected the antenna return loss performance.

Figures 23(a) and (b) show the comparison of the simulated and measured radiation pattern for the 4×1 array in elevation plane (E-plane) and azimuth plane (H-plane), respectively. The designed antenna produces a gain of 12.4 dB and 13.78 dB for simulated and measured results, respectively, with a difference of 1.38 dB only. The polar plot results reach a reasonable agreement for both simulation and measurement. The measured efficiency was reduced from 82.55% during simulation to 68.71%; however, the value is still acceptable. The slight degradation of efficiency is due to the losses caused by the slight misalignment during radiation pattern measurement.

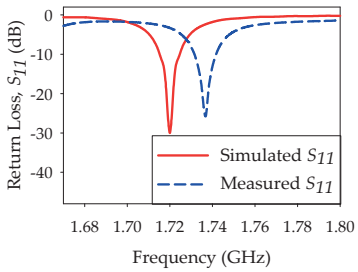

Fig. 22. The simulated and measured return loss of the 4×1 array.

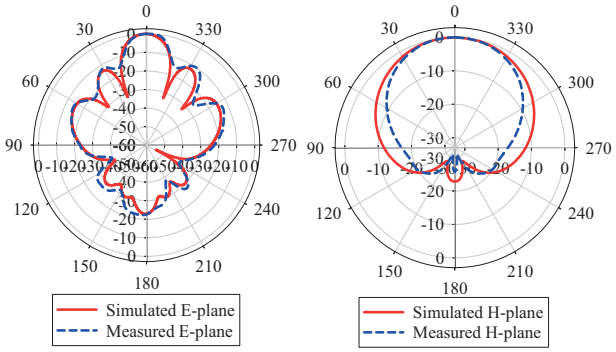

Fig. 23. Simulated and measured radiation pattern of 4×1 array: (a) E-plane, and (b) H-plane.

4.2.2 Convex Bent Array

Figures 24(a) and (b) show the simulated and measured return loss and E-plane radiation pattern of the convex bent array antenna. The measured resonant frequency was slightly shifted from 1.72 GHz to a higher frequency of 1.736 GHz with about a 0.93% difference. The shifting of resonant frequency might be due to the losses from the SMA connector used during the arrangement setup of the measurement process. However, the return loss result for both simulation and measurement is still good since it is still within the base station operating band range. A good agreement for the simulated and measured bandwidth is obtained, 9.46 MHz and 9.59 MHz, respectively. The E-plane radiation pattern for a convex bent array antenna in the polar plot is shown in Fig. 24(b). Both measured and simulated results seem to have an excellent bifurcated beam performance, with the simulated and measured gain of 7.62 dB and 7.36 dB, respectively. However, the back lobe of the measured radiation pattern is more significant than the simulation due to the reflections from cables inside the anechoic chamber and misalignment during measurement. The simulated and measured efficiency is 81.81% and 74.30%, showing a slight degradation. As expected, the shifting angle, θ_s of the bifurcated beam, is 38.50°, which indicates that the desired θ_s were not achieved for this design, as shown by (4).

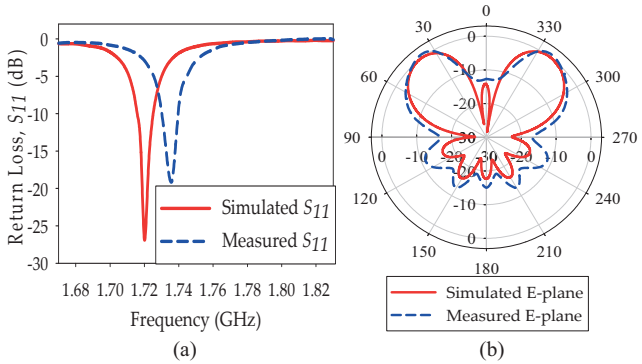

Fig. 24. Simulated and measured results of a convex bent array: (a) return loss, and (b) E-plane radiation pattern.

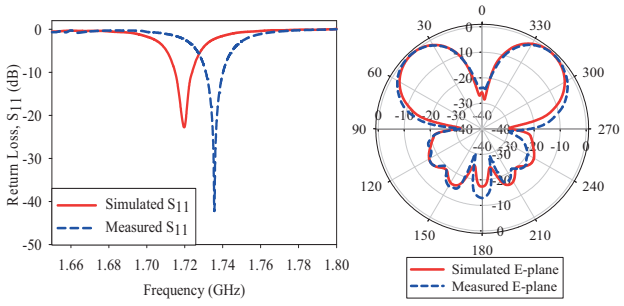

Fig. 25. Simulated and measured results of an extended convex bent array; (a) return loss, and (b) E-plane radiation pattern.

4.2.3 Extended Convex Bent Array

The simulated and measured return loss of an extended convex bent array is shown in Fig. 25(a). The measured resonant frequency is slightly shifted to about 0.016 GHz from the desired frequency. However, it is still acceptable with only about 0.93% in terms of percentage difference. It might be due to fabrication tolerance, especially during the cable and antenna assembly. The frequency shifting also happened might be due to the fabricated material used. Thus, the value of ε_r needs to be remeasured before the fabrication process to ensure that the ε_r value is the same as the simulation material used during the antenna design. However, the bandwidth results are almost similar, with 9.34 MHz and 9.75 MHz for measurement and simulation.

The simulated and measured bifurcated beam radiation pattern in E-plane was plotted in a graph as shown in Fig. 25(b). Both results show good radiation patterns, which indicate that the signal radiates in two main directions to obtain the bifurcated beam. It is clearly demonstrated that the antenna has a balance radiation signal for both sides of bifurcated beams. The maximum simulated gain of the extended convex bent array antenna is 7.32 dB, while the measured gain is 6.98 dB. The measured antenna efficiency has decreased by about 4.27%, from 81.46% to 77.98%.

5. Conclusion

This study proposed a convex bent array antenna design to produce an optimum bifurcated beam radiation pattern for a cylindrical lens antenna. A 4×1 array with a serial feed line network has been designed to produce a balanced and uniform bifurcated beam. Besides that, the optimum array excitation for each radiating element was also performed by optimizing the serial feedline. Then, a convex bent array was developed and produced an excellent bifurcated beam radiation pattern. However, the θ_s of this bifurcated beam were smaller than the targeted value derived by (2). Then, the dimension parameters of the substrate and ground planes were extended using the fringing

effect concept. By this extension, the θ_s were increased by about 10.39%, and it is concluded that the bifurcated beam shifting angle can be increased using this method. Besides that, the extended convex bent array antenna showed better performance, based on the smaller middle lobe between the bifurcated beams than the non-extended version. The reliability and validity of the proposed bifurcated beam for efficient lens illumination are verified based on the aperture distribution results. Based on the analysis, the extended convex bent array with $d = 0.7\lambda_o$ is demonstrated to produce better aperture distribution with high lobe magnitude, indicating efficient illumination at the lens surface. The technical performance of the 4×1, convex bent, and the extended convex bent array was validated through fabrication and measurement works. The simulated and measured results show good agreement.

Acknowledgments

The authors would like to thank all the researchers involved in this research, mainly from the Antenna Research Centre, School of Electrical Engineering, College of Engineering, Universiti Teknologi MARA (UiTM), Shah Alam, Selangor, Malaysia. This work was sponsored by UiTM under Young Talent Researcher Grant (YTR) with reference no. 600-RMC/YTR/5/3(012/2020).

References

[1] WANG, W., LIU, A., ZHANG, Q., et al. Robust multigroup multicast transmission for frame-based multibeam satellite systems. *IEEE Access*, 2018, vol. 6, p. 46074–46083. DOI: 10.1109/ACCESS.2018.2865998

[2] HASSAN, W. A., JO, H. S., THAREK, A. R. The feasibility of coexistence between 5G and existing services in the IMT-2020 candidate bands in Malaysia. *IEEE Access,* 2017, vol. 5, p. 14867 to 14888. DOI: 10.1109/ACCESS.2017.2690309

[3] SAADA, M. H. A. Design of efficient millimeter wave planar antenna for 5G communication systems. *M. S. Thesis,* The Islamic University of Gaza, 2017. DOI: 10.13140/RG.2.2.13540.37760

[4] RAHIMA, S. K. A., HAKIMI, S., YAMADA, Y., et al. Investigation of pencil and bifurcated beam fed cylindrical dielectric lens antenna for 5G mobile base stations. *Journal of Telecommunication, Electronic and Computer Engineering,* 2017, vol. 9, no. 1–5, p. 27–32. ISSN 2180-1843

[5] AHMADI, S. Toward 5G Xilinx solutions and enablers for next-generation wireless systems. *White Paper: Xilinx MPSoCs and FPGAs,* 2016, vol. 1, p. 1–32. Available at: https://docs.xilinx.com/v/u/en-US/wp476-toward-5g

[6] TENGAH, Z., ALI, M. T., ABD RAHMAN, N. H., et al. Achievement of a bifurcated beam by a bend-array configuration. In *Proceedings of the 2016 6th IEEE-APS Topical Conference on Antennas and Propagation in Wireless Communications.* Cairns (Australia), 2016, p. 1–4. DOI: 10.1109/APWC.2016.7738137

[7] TANAKA, M., NAKAMURA, M., KAWAI, M., et al. Experimental fixed and mobile multibeam satellite communications system. In *IEEE International Conference on Communications.* Boston (USA), 1989, p. 1–8. DOI: 10.1109/ICC.1989.49945

[8] PARCHIN, N. O., SHEN, M., PEDERSEN, G. F. Small-size tapered slot antenna (TSA) design for use in 5G phased array applications. *ACES Journal,* 2017, vol. 32, no. 3, p. 193–202. ISSN: 1943-5711

[9] OJAROUDIPARCHIN, N., SHEN, M., PEDERSEN, G. F. A 28 GHz FR-4 compatible phased array antenna for 5G mobile phone applications. In *2015 International Symposium on Antennas and Propagation (ISAP).* Hobart (TAS, Australia), 2015, p. 1–4. ISBN: 978-4-8855-2302-1

[10] HUANG, F., CHEN, W., RAO, M. Switched-beam antenna array based on Butler matrix for 5G wireless communication. In *2016 IEEE International Workshop on Electromagnetics: Applications and Student Innovation Competition (iWEM).* Nanjing (China), 2016, p. 1–3. DOI: 10.1109/iWEM.2016.7505030

[11] MOODY, H. The systematic design of the Butler matrix. *IEEE Transactions on Antennas and Propagation,* 1964, vol. 12, no. 6, p. 786–788. DOI: 10.1109/TAP.1964.1138319

[12] ROTMAN, W., TURNER, R. Wide-angle microwave lens for line source applications. *IEEE Transactions on Antennas and Propagation,* 1963, vol. 11, no. 6, p. 623–632. DOI: 10.1109/TAP.1963.1138114

[13] ANSARUDIN, F., ABD RAHMAN, N. H., YAMADA, Y., et al. Multi beam dielectric lens for 5G base station. *Sensors,* 2020, vol. 20, no. 20, p. 1–17. DOI: 10.3390/s20205849

[14] GIDDENS, H., HAO, Y. Multi-beam graded dielectric lens antenna from multi-material 3D printing. *IEEE Transaction on Antennas and Propagation,* 2020, vol. 68, no. 9, p. 6832–6837. DOI: 10.1109/TAP.2020.2978949

[15] YAMADA, Y., QUZWAIN, K. M. C., IDRUS I. I., et al. Base station antennas for the 5G mobile system. In *Proceeding of 2018 IEEE International RF and Microwave Conference (RFM).* Penang (Malaysia), 2018, p. 1–4. DOI: 10.1109/RFM.2018.8846489

[16] LO, Y. T., LEE, S. W. *Antenna Handbook, Volume III, Antenna Applications.* Chapman & Hall, 1993. ISBN: 978-0442015947

[17] ANSARUDIN, F., ABD RAHMAN, T., YAMADA, Y. Design of dielectric lens antenna for 5G mobile base station. In *2018 International Symposium on Antennas and Propagation (ISAP 2018).* Busan (South Korea), 2018, p. 1–2. ISBN: 978-89-5708-304-8

[18] HUNG, P. V., DINH, N. Q., YAMADA, Y., et al. Parametric analysis of negative and positive refractive index lens antenna by ANSYS HFSS. *International Journal of Antennas and Propagation (Hindawi),* 2020, vol. 2020, p. 1–11. DOI: 10.1155/2020/9128921

[19] BALLESTEROS, C., MAESTRE, M., SANTOS, M. C., et al. A 3D printed lens antenna for 5G applications. In *Proceedings of the 2019 IEEE International Symposium on Antennas and Propagation and USNC-URSI Radio Science Meeting,* Atlanta (GA, USA), 2019, p. 1985–1986. DOI: 10.1109/APUSNCURSINRSM.2019.8889092

[20] LI, Y., GE, L., CHEN, M., et al. Multibeam 3-D-printed Luneburg lens fed by magnetoelectric dipole antennas for millimeter-wave MIMO applications. *IEEE Transactions on Antennas and Propagation.* 2019, vol. 67, no. 5, p. 2923–2933. DOI: 10.1109/TAP.2019.2899013

[21] COMISSO, M., PALESE, G., BABICH, F., et al. 3D multibeam and null synthesis by phase-only control for 5G antenna arrays. *Electronics,* 2019, vol. 8, no. 6, p. 656–669. DOI: 10.3390/electronics8060656

[22] WANG, Z. X., DOU, W. B. Design and analysis of several kinds of dielectric lens antennas. *Journal of Electromagnetic Waves and Application,* 2006, vol. 20, no. 12, p. 1643–1653. DOI: 10.1163/156939306779292327

[23] KOMLJENOVIC, T. *Lens Antenna - Analysis and Synthesis at mm-Waves.* Faculty of Electrical Engineering and Computing, University of Zareb, 2008. Available at: https://citeseerx.ist.psu.edu/viewdoc/download?doi=10.1.1.525.8224&rep=rep1&type=pdf

[24] ZHANG, Z., YANG, S., ZENG, Y., et al. A cylindrical lens antenna with extremely flat beams. *IEEE Access,* 2019, vol. 7, p. 156675–156685. DOI: 10.1109/ACCESS.2019.2948961

[25] BALANIS, C. A. *Antenna Theory: Analysis and Design.* 3rd ed. Hoboken (New Jersey, Canada): John Wiley & Sons, Inc., 2005, p. 14–20. ISBN: 978-0-471-66782-7

[26] STUTZMAN, W. L., THIELE, G. A. *Antenna Theory and Design.* 2nd ed. United States: John Wiley & Sons, Inc., 1998, p. 130–137. ISBN: 0-471-02590-9

[27] ABD RAHMAN, N. H., YAMADA, Y., NORDIN, M. S. A. Analysis on the effects of the human body on the performance of electro-textile antennas for wearable monitoring and tracking application. *Materials,* 2019, vol. 12, no. 10, p. 1–17. DOI: 10.3390/ma12101636

[28] WOO, H., KHAN, A. R., MASUI, H., et al. Discharge observation on antenna surface radiating high power microwave in plasma environment. *Transactions of the Japan Society for Aeronautical and Space Sciences, Aerospace Technology Japan,* 2014, vol. 12, p. 11–19. DOI: 10.2322/tastj.12.11

[29] TENGAH, Z., ALI, M. T., ABD RAHMAN, N. H., et al. Design of serial feeds for a bifurcated beam of bend-array configuration. In *2016 IEEE Asia-Pacific Conference on Applied Electromagnetics (APACE).* Langkawi (Malaysia), 2016, p. 43–46. DOI: 10.1109/APACE.2016.7916471

[30] YASIN, S., KHUDA, I. E., NAZIR, I., et al. Numerical modeling of the order of convergence of surface charge density useful in estimating bandwidth for microstrip patch antenna. *Asian Journal of Engineering, Sciences & Technology,* 2015, vol. 5, no. 2, p. 1–3. Available at: https://www.researchgate.net/publication/325010282

[31] SMOLDERS, B., VAATE, J. G., KANT, D., et al. *Dual-Beam Wideband Beamformer with Integrated Antenna Array*. University of Massachusetts, Amherst, USA, 2000. Available at: https://www.researchgate.net/publication/228358713

[32] https://www.mathworks.com/products/matlab.html

[33] https://rfstation.com/cst/

[34] PIKSA, P., ZVANOVEC, S., CERNY, P. Elliptic and hyperbolic dielectric lens antennas in mm-waves. *Radioengineering,* 2011, vol. 20, no. 1, p. 270–275. ISSN: 1210-2512

[35] LO, Y. T., LEE, S. W. *Antenna Handbook. Volume II.* Van Nostrand Reinhold, New York, 1994. ISBN: 978-0442015930

About the Authors ...

Zanurlida TENGAH was born in Terengganu, Malaysia, in 1988. She received B.Eng degree in Electronics (communication) from Universiti Teknologi MARA (UiTM) Shah Alam, Selangor, Malaysia, in 2012. In 2014, she received her M.Sc. degree in Telecommunication and Information Engineering from the same university. She also has experience working as Under Postgraduate Teaching Assistant in UiTM. Currently, she is pursuing her Ph.D. degree in Electrical Engineering at Universiti Teknologi MARA (UiTM) Shah Alam, Selangor, Malaysia. Her research interests are array antennas, lens antennas, and electromagnetic waves applications.

Nurul Huda ABD RAHMAN (corresponding author) (M'15) received her M.Eng degree in Electronics from the University of Surrey, Guildford, the United Kingdom, in 2008 and a Ph.D. degree in Electric, Electronic, and Systems Engineering from Universiti Kebangsaan Malaysia in 2014. She joined Astronautic Technology (M) Sdn. Bhd. as a Spacecraft Engineer in 2008, where she was involved in various small-class satellite development and R&D projects. In 2014, she was appointed as a Senior Lecturer in Universiti Teknologi MARA Malaysia (UiTM) and has been working in the same university until now. She also received a 2-year Postdoctoral Fellowship under the Malaysia-Japan International Institute of Technology, Universiti Teknologi Malaysia between 2018–2019. Her current research interests include antennas for space and terrestrial applications, array antennas, reflector and lens antennas, wearable and flexible antennas, RF and microwave design, and electromagnetic analysis. She has been the Professional Engineer of the Board of Engineers Malaysia (BEM) since 2019. She has been appointed as the Executive Committee of the IEEE Malaysia AP/MTT/EMC Joint Chapter for 2021–2022. She was also the recipient of the Best Professional Paper Award IEEE Malaysia Comsoc & VTS Joint Chapter in 2018 and the Best Paper Award from IEEE Malaysia AP/MTT/EMC Joint Chapter in 2018 and 2019.

Yoshihide YAMADA received his bachelor's and Master of Engineering from Nagoya Institute of Technology in 1971 and 1973, respectively. And he received the Dr. of Electrical Engineering from the Tokyo Institute of Technology in 1989. He joined Electrical Communication Laboratories of Nippon Telegraph and Telephone Corporation (NTT) in 1973 and moved to NTT Mobile Communications Network Inc. (NTT DoCoMo) in 1993. In 1998, he joined the National Defense Academy as a Professor. In 2014, he joined the Malaysia-Japan International Institute of Technology of UTM, Malaysia as a Professor. He is a Fellow of IEICE Japan, a senior member of IEEE APS and a member of ACES. His research interests are aperture antennas, array antennas, very small antennas, and radar cross-sections. He received the excellent paper award and the tutorial paper award from IEICE in 2013 and 2014, respectively.

Nur Emileen ABD RASHID is currently an Associate Professor at University Teknologi MARA. She obtained the Bachelor of Electrical Engineering (Telecommunication Engineering) from Universiti Kebangsaan Malaysia in 2001 and subsequently her MSc. in Computer, Communication and Human-Centered Engineering from the University of Birmingham, the UK in 2002. She pursued her studies and received her Ph.D. in 2011 from the same university. She has contributed much expertise in Radar Technology, telecommunications signal processing, RF design, and clutter modeling. Currently, she is attached to the Microwave Research Institute as a member and appointed as Head of Resources. Dr. Nur Emileen is an active member of IET, IEEE and MyRAN.

Idnin PASYA is a member of the Microwave Research Institute and the Faculty of Electrical Engineering, Universiti Teknologi MARA. He received his B. E. and M. E. in Information and Communication Engineering from Tokyo Denki University in 2004 and 2006, respectively, and his Ph.D. in Communication Engineering from the same university in 2015. Previously, he worked as an Engineer in Toshiba PC & Network, Tokyo, Japan, from 2006 to 2009, and Pradonet Technology Sdn. Bhd. as Senior Product Engineer in 2009, before joining UiTM in the same year. He contributed to IEEE as an executive committee for IEEE AP/MTT/EMC Joint Chapter for 2017–2020. He is also an active member of the SIRIM Technical Committee on "Electromagnetic Field" (TC/E/6) for 2016–2020. His current research areas are wideband antennas and communication systems, underwater EMW propagation and communication, and MIMO radar and its applications. He received the IEEE MTT Best Paper Award in the 2014 IEEE Radio and Wireless Symposium, held in California, USA.

Mohd Aziz ARIS was born in Sabah Malaysia in 1975 and is a Senior Lecturer in Universiti Teknologi MARA Terengganu and joint UiTM since 2006. He received a B.Eng. degree in Electrical Engineering (Telecommunication) from the Universiti Teknologi MARA (UiTM), Shah Alam Selangor. In 2000, he received the M.Sc. degree in Telecommunication and Information Engineering by research from the Universiti Teknologi MARA (UiTM), Shah Alam, Malaysia, in 2006. He completed his Ph.D. in Electrical Engineering (Telecommunication) from the Universiti Teknologi MARA (UiTM), Shah Alam Selangor, in 2017. His research interests include communication antenna design such as reconfigurable microstrip antennas, array antennas, electromagnetic radiation analysis, and indoor/outdoor propagation modeling.

Nguyen Quoc DINH is currently an Associate Professor at the Faculty of Radio-Electronics Engineering, Le Quy Don Technical University Vietnam. He received the B.E, M.E., and D.E. degrees in the Department of Electrical & Electronic Engineering, National Defense Academy, Yokosuka, Japan, in 2006, 2008, and 2011, respectively. Since 2011, he has been a Research Associate at the Faculty of Radio-Electronics Engineering, Le Quy Don Technical University, Hanoi, Vietnam. His research interests include very small antennas, array antennas, UWB antennas, MIMO antennas, and BTS antennas. He is a member of the Institute of Electronics, Information and Communication Engineers (IEICE), Japan and the recipient of the Young Scientist Award of the IEICE Antennas and Propagation Society Japan Chapter, Japan (2011).